

Global Modeling Organics-related New Particle Formation and its Contribution to Global Aerosol Number Concentrations using CAM6-Chem

Text S1. Ion Concentrations in CAM6-Chem

Ions are introduced to the model to simulate ion-induced NPF (Dunne et al., 2016). Specifically, we consider atmospheric ions generated by galactic cosmic rays. The ion concentrations, denoted as $[n_{\pm}]$, are computed following the equation outlined by Franchin et al. (2015):

$$[n_{\pm}] = \frac{(k_i^2 + 4\alpha q)^{0.5} - k_i}{2\alpha} \quad (S1)$$

and q ($\text{cm}^{-3} \text{ s}^{-1}$) represents the ion-pair production rate by galactic cosmic rays (download from: <https://svn-ccsm-inputdata.cgd.ucar.edu/trunk/inputdata/atm/waccm/gcrs/>). α is the ion-ion recombination coefficient ($\text{cm}^3 \text{ s}^{-1}$) calculated by (Franchin et al., 2015):

$$\alpha = 6 \times 10^{-8} \left(\frac{300}{T}\right)^{0.5} + 6 \times 10^{-26} [M_{air}] \left(\frac{300}{T}\right)^4 \quad (S2)$$

$[M_{air}]$ is the concentration of air molecules (cm^{-3}). The ion loss rate k_i , is due to the ion condensation sink (CS) onto aerosols and the ion-induced nucleation:

$$k_i = CS + \frac{J_{org,i}}{2[n_{\pm}]} \quad (S3)$$

Text S2. COC Saturated Concentration in CAM6-Chem

Condensable organic compounds (COC) condense onto newly formed aerosols in accordance with their saturation vapor concentration, denoted as (C_{COC}^*) . This concentration is computed using the ideal gas law equation:

$$C_{COC}^* = \frac{MW \times \zeta \times P(T)}{R T} \quad (S4)$$

where MW is the molecular weight of the COC and ζ is the activity coefficient of COC and assumed equal to 1. $P(T)$ is the saturation vapor pressure at temperature T , R is the ideal gas constant. The saturation vapor pressure at temperature T can be calculated following Chung and Seinfeld (2002):

$$P(T) = P(T_0) \cdot e^{\left[\frac{-\Delta H_{vap}}{R} \left(\frac{1}{T} - \frac{1}{T_0}\right)\right]} \quad (S5)$$

34

where $P(T_0)$ is the saturation vapor pressure at temperature $T_0 = 298$ K and ΔH_{vap} is the enthalpies of vaporization which represent the energy to transform the liquid substance into gas-phase (values shown in Table 1).

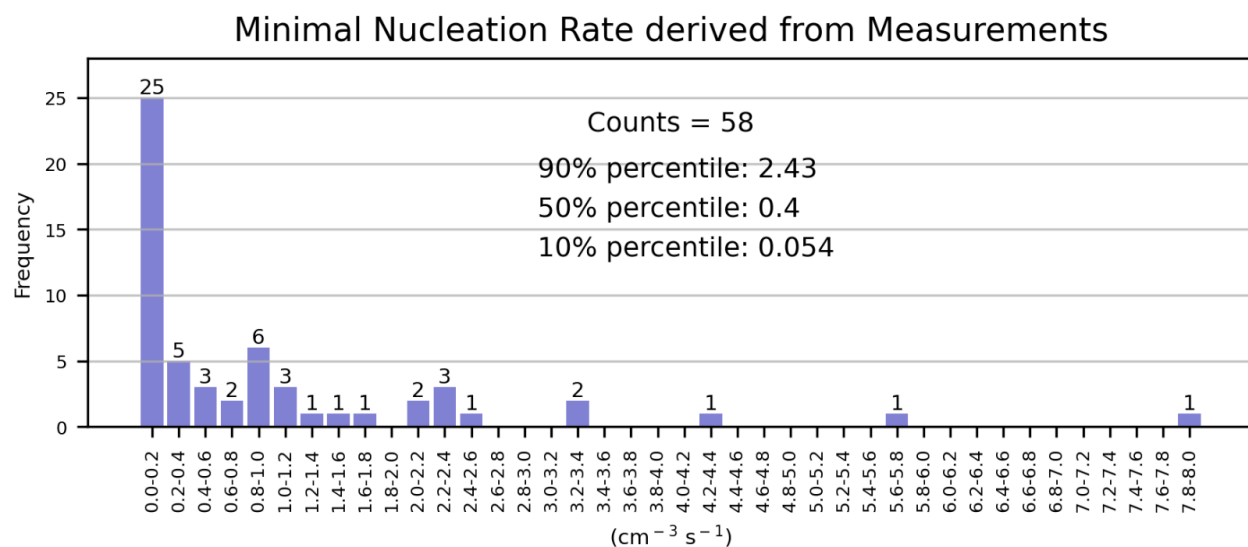
36

38 Text S3. Threshold Value of NPF Event Happening

40 To determine the threshold to initiate an NPF event (i.e., the threshold of j_{20nm} in model), we collect smallest nucleation rates (at size between 5nm to 30nm) measurements in Kerminen et al. (2018). Following Kerminen et al. (2018), there are total 58 sites showing smallest nucleation rates with different backgrounds, including boreal forest, China, mountainous regions, polars, rural remote and urban regions (<https://iopscience.iop.org/article/10.1088/1748-9326/aadf3c/data>). Distribution of frequency of the smallest nucleation rates that instrument can detect from different stations are shown in Figure S1.

46 When $j_{20nm} >$ threshold, we can compare simulated nucleation / growth rate during NPF events (Table S1), condensation sink and NPF frequency (Table S2) with measurements, even in stations where thresholds are not detectable. We chose 10th percentile ($j_{20nm} = 0.054 \text{ cm}^{-3} \text{ s}^{-1}$), median value ($j_{20nm} = 0.4 \text{ cm}^{-3} \text{ s}^{-1}$) and 90th percentile ($j_{20nm} = 2.43 \text{ cm}^{-3} \text{ s}^{-1}$) of all smallest nucleation rates (Figure S1) as the threshold individually. This helps us to quantify uncertainty in above-mentioned simulated parameters (shown in Table S1 and S2).

50

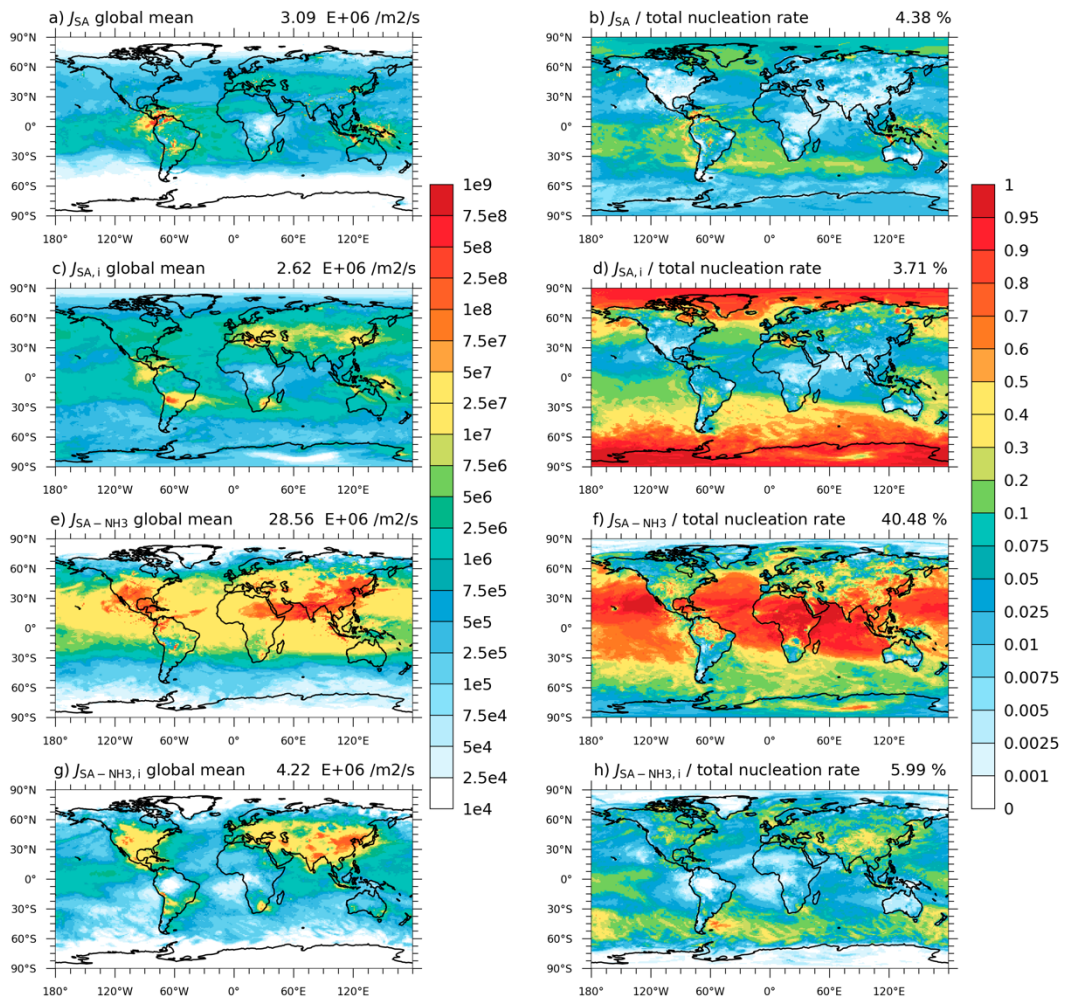


52

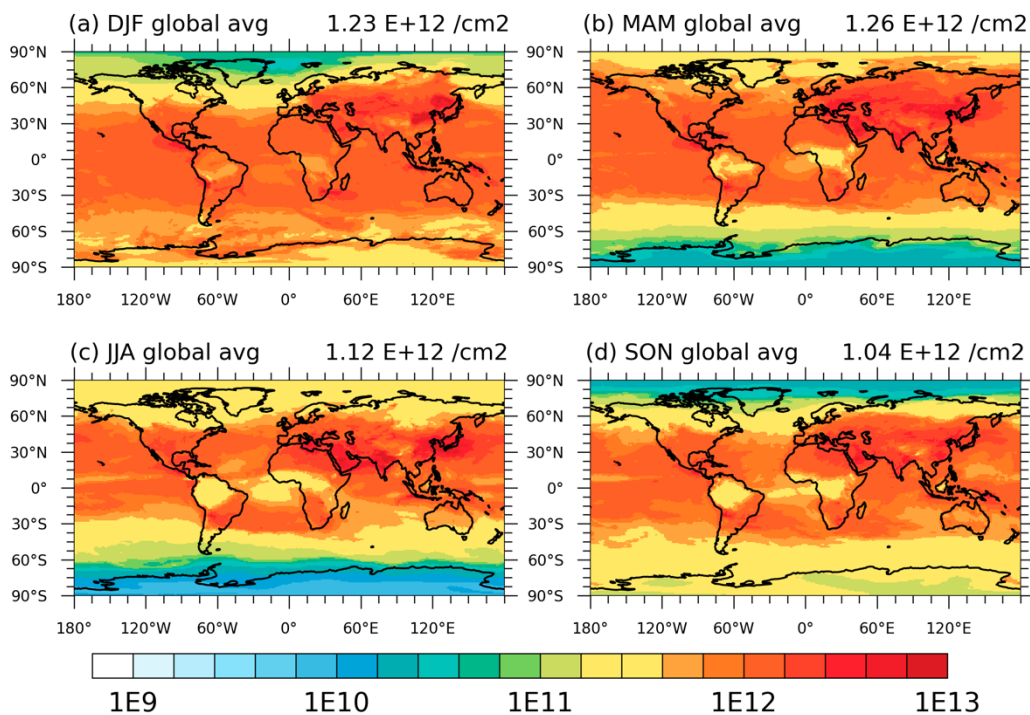
Figure S1. Frequency of smallest nucleation rate could 'start' NPF events. All the smallest nucleation rate values derived from Kerminen et al. (2018). Counts and different percentiles of all the collected nucleation rates are texted in figure.

54

56



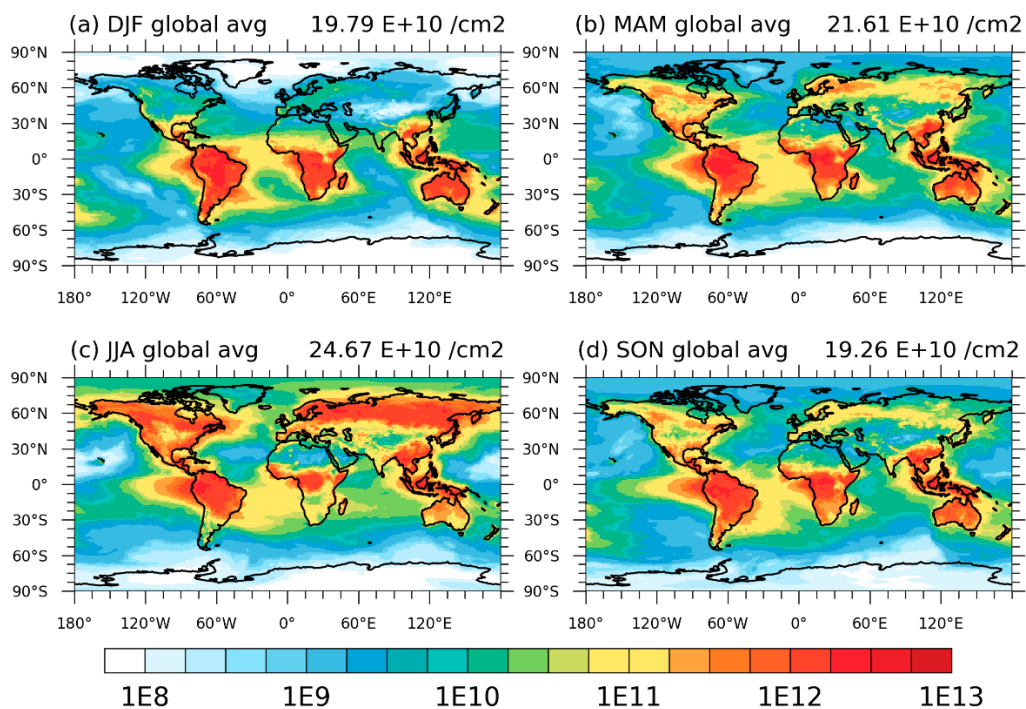
58 Figure S2. The 2013 annual average vertically integrated organic nucleation rate in the troposphere (a, c, e, g) and their contribution (b, d, f, h)
 60 for binary neutral nucleation (a, b), binary ion-induced nucleation (c, d), ternary neutral nucleation (e, f), and ternary ion-induced nucleation (g, f) for the Inorg_Org case. The strings at the upper right indicate the global mean value.



62

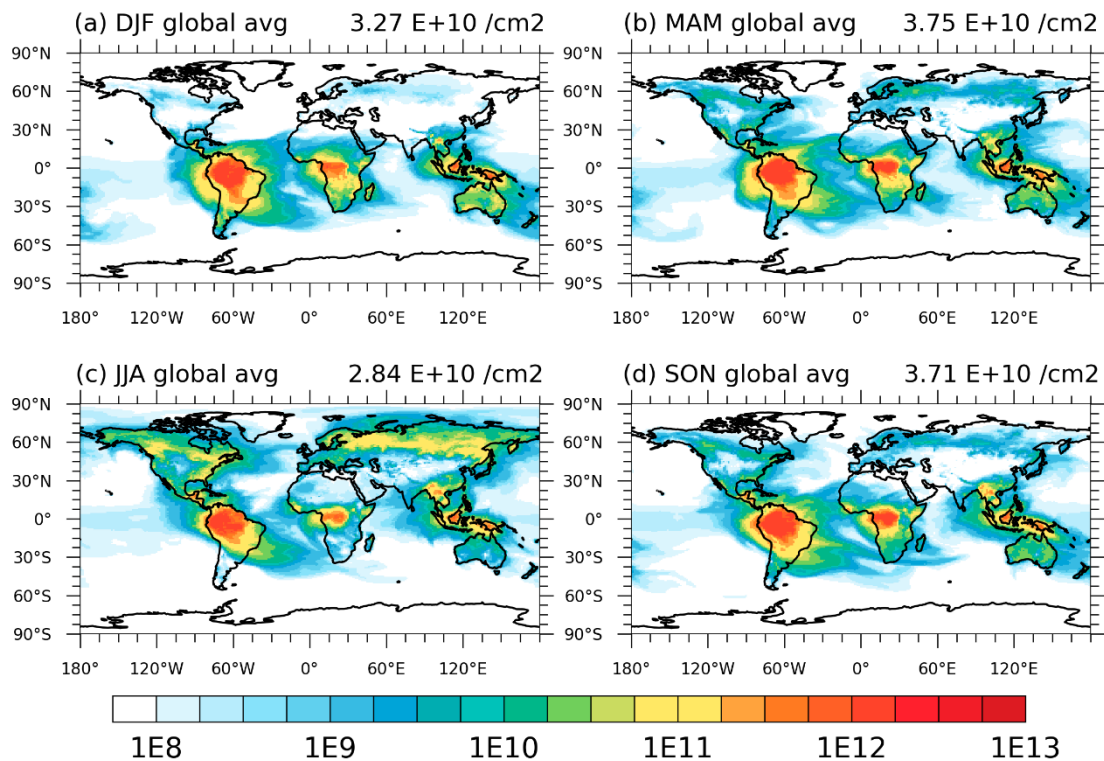
64 Figure S3. The 2013 annual average vertically integrated H_2SO_4 concentration for (a) DJF, (b) MAM, (c) JJA, and (d) SON in the Inorg_Org (Units: cm^{-2}). The strings at the upper right indicate the global mean value.

66



68

70 Figure S4. The 2013 annual average vertically integrated HOMs concentration for (a) DJF, (b) MAM, (c) JJA, and (d) SON in the Inorg_Org (Units: cm^{-2}). The strings at the upper right indicate the global mean value.

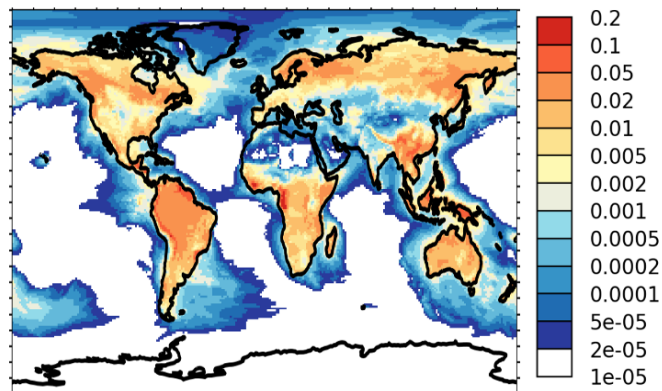


72

Figure S5. The 2013 annual average vertically integrated ACC concentration for (a) DJF, (b) MAM, (c) JJA, and (d) SON in the Inorg_Org (Units: cm⁻²). The strings at the upper right indicate the global mean value.

74

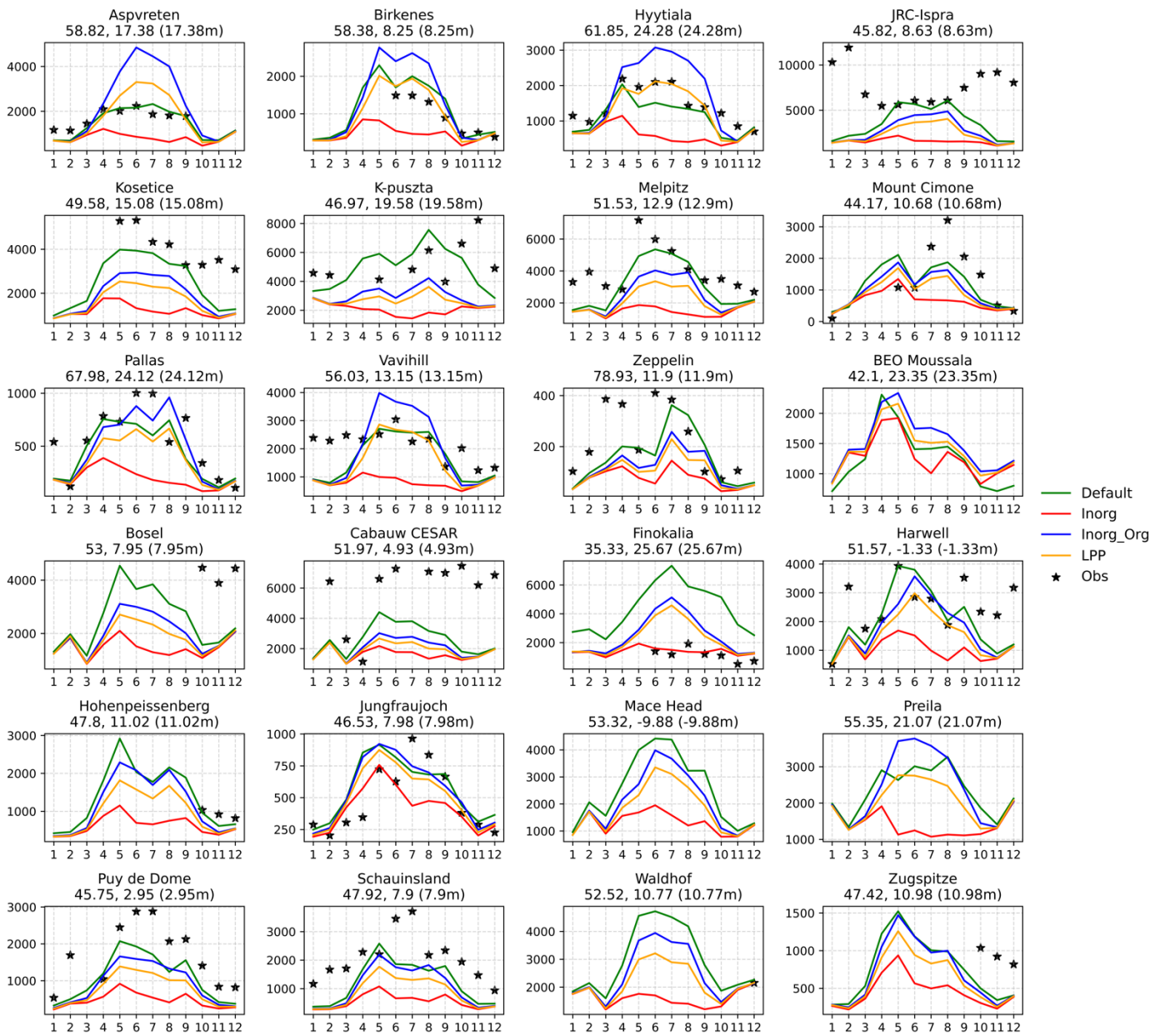
76



78

Figure S6. Annually averaged concentrations of HOMs at the top of boundary layer concentrations in this study in 2013 (scaled by 1/10) (Units: pptv).

80

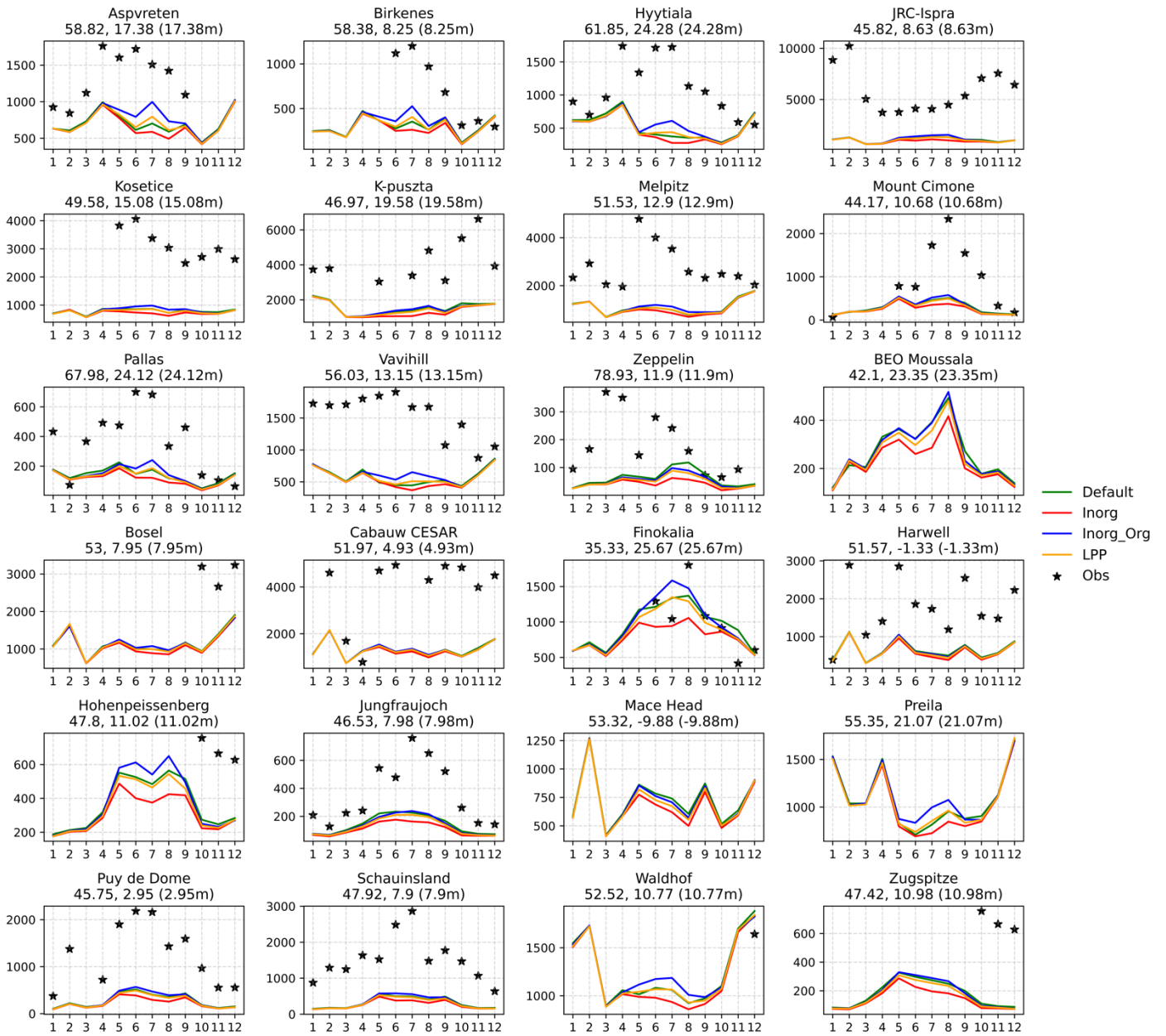


82

84

86

Figure S7. Seasonal cycle of N30 in 2008 at EUARCCI measurement sites (Units: cm^{-3}). The subtitle indicates site locations. Solid stars represent measured monthly mean concentrations. Numbers in X-axis show the month. Model experiments are detailed in Table 2. The red line depicts the default CESM2.1 model (Default), the yellow line indicates the model with an updated inorganic nucleation scheme (Inorg), blue lines represent the model incorporating organic nucleation based on Inorg (Inorg_Org), and orange lines are similar to blue lines but utilize a lower mass yield for nucleating organics (LPP).



88

90

Figure S8. Same as Figure S6, but for N50 (unit: cm^{-3})

Table S1. Results of model simulations conducted at 13 different sites, based on the experimental configurations outlined in Table 2.

Date	Station ^c	Location	Type	Nucleation Rate (J) (/cm ³ /s)			Size for J (nm)	Growth Rate (GR) (nm/h)			Size range for GR (nm)
				Obs ^a	Inorg_Org ^b	Inorg ^b		Obs ^a	Inorg_Org ^b	Inorg ^b	
03-04/2007	Hyytiälä, Finland	61.51° N, 24.17° E (181m)	Boreal	1.08±1.05	2.4 ~ 4.3 (2.6)	0.3 ~ / (0.8)	[3, 40]	2.76±0.9	7.4~11.9 (8.1)	3.0~/ (3.8)	[3, 40]
08-10/2012	Ozark Forest, US	38.74° N, 92.20° W (3.7m)	Forest	11±10.6	5.3 ~ 10.8 (6.1)	0.4 ~ / (0.9)	1	4.7±2.6	5.6~6.8 (6.0)	5.9 ~ / (5.4)	[5, 25]
06/2012	Po Valley, Italy	44.39° N, 11.37° E (11m)	Rural	6.8 (2.7~38.5)	3.0 ~ 4.2 (3.1)	/	[2.7, 38.5]	7.2 (3.8~13.8)	10.7~14.3 (11.1)	/	[7, 20]
03-06/2014	Leicester, UK	52° 37' N, 1° 07' W	Urban	1.335	2.7 ~4.5 (3.0)	0.3 ~ / (0.8)	[10, 25]	1.3±0.4	6.2~7.8 (6.5)	8.2~/ (9.8)	[10, 25]
08/2007	Toronto, Canada	43° 42' N, 79° 32' W	Semi-urban	12.9	8.2 ~ 14.4 (9.2)	0.2 ~ / (0.9)	[5.6, 30]	6.3±1.6	8.6~9.5 (9.0)	13.7 ~ / (12.6)	[5.6, 30]
04-07/2012	Gadanki, India	13.46° N, 79.17° E (375m)	Semi-urban	1.2±2.3	1.2 ~ / (1.6)	/	[5, 25]	4.1±2	5.5~/ (5.8)	/	[5, 25]
09-11/2015	Nanjing, China	32.30° N, 118.72° E	Urban	7±3.89	1.6 ~ / (2.5)	/	[5,10]	6.2±2.6	10.5~/ (12.1)	/	[10, 20]
06-07/2014	Wangdu, China	38.67° N, 115.21° E	Rural	24.6±22.8	3.2 ~ 7.5 (4.1)	/	[3, 25]	7.3±3.3	9.7~13.1 (10.7)	/	[3, 25]
07/2008	Beijing, China	39.56° N, 116.19° E (35 m)	Urban	No Obs	5.9 ~ / (7.0)	0.1 ~ / (/)	1.7	6.9±2.7	12.9~11.2 (13.9)	29.7~/ (/)	[12, 550]
01-03/2012	Nanjing, China	32.12° N, 118.95° E	Urban	23.9 (2.6-56.8)	0.5 ~ / (/)	0.4 ~ / (/)	2	5.9 (6.1-10.9)	5.3~/ (/)	4.8~/ (/)	[3, 7]
04-05/2010	Qingdao, China	36° 09' N, 120° 29' E	Urban/Coast	13.8±14.8	4.4 ~ 11.0 (5.6)	0.1 ~ / (/)	[5.6, 30]	6.4±2.2	11.2 ~ 11.4 (11.4)	10.5~/ (/)	Over the growth period
10-11/2010	Hongkong, China	22.41° N, 114.12° E (640m)	Suburban	2.95±2.1	0.3 ~ / (/)	0.3 ~ / (/)	[5.5, 10]	3.9±1.9	14.4 ~ / (/)	14.2~/ (/)	[5.5, 25]
12/2010-01/2011	Hongkong, China	22.3° N, 114.18° E (40m)	Urban	1.9±0.6	/	/	[5.5, 10]	5.2±1.6	/	/	[5.5, 10]

^aObs represents mean value from observation from measurements

^bThe model result is presented as a range for each site: the lower limit of the range is mean value of nucleation/growth rate during NPF event when choosing the 10th percentile of all smallest nucleation rates as the threshold ($j_{20nm} = 0.054 \text{ cm}^{-3} \text{ s}^{-1}$) of NPF event happening, while the upper limit is based on the 90th percentile. Values in brackets represent results obtained using the median as the threshold value. A forward slash (/) indicates that no NPF events were detected in the simulation.

^cMeasurements in Hyytiälä are from Pierce et al. (2011). Measurements in Ozark forest are from Yu et al. (2014). Measurements in Po Valley are from Kontkanen et al. (2016). Measurements in Leicester are from Hama et al. (2017). Measurements in Toronto are from Meng et al. (2015). Measurements in Gadanki are from Kanawade et al. (2014). Measurements in Nanjing (2015) are from Dai et al. (2017). Measurements in Wangdu are from Wu et al. (2017). Measurements in Beijing are from Zhang et al. (2011). Measurements in Nanjing (2012) are from Herrmann et al. (2014). Measurements in Qingdao are from Zhu et al. (2014). Measurements in Hongkong (2010) are from Guo et al. (2014). Measurements in Hongkong (2010-2011) are from Wang et al. (2015).

Table S2. Comparison between measured and modeling NPF frequency and condensation sink during NPF events. Model experiments are described in Table 2.

Date	Station ^d	Location	Type	NPF Frequency (%)			Condensation Sink (s-1)		
				Obs	Inorg_Org	Inorg	Obs	Inorg_Org	Inorg
04-05/2007	Pallas, Finland	67° 58' N, 24° 07' E (560m)	Boreal forest	20	0	0	0.63	No event	No event
04-05/2007	Hyytiälä, Finland	61° 50' N, 24° 18' E (180m)	Rural, boreal forest	48	36~54 (49)	0~15 (0)	1.4	2.3 ± 1.1	No event
04-05/2007	Vavihill, Sweden	56° 01' N, 13° 09' E (172m)	Rural	57	41~61 (57)	0~13 (0)	3.4	3.2 ± 1.2	1.9 ± 1.3
04-05/2007	Mace Head, Ireland	53° 19' N, 09° 53' W (5m)	Atlantic, bare land	/	13~43 (39)	0~5 (0)	0.64	4.8 ± 1.4	1.6 ± 0.1
04-05/2007	Cabauw, Netherlands	51° 57' N, 04° 53' E (0m)	Ocean/urban	65	5~20 (18)	0~8 (0)	2.9	2.2 ± 0.8	1.0 ± 0.2
04-05/2007	Melpitz, Germany	51° 32' N, 12° 54' E (87m)	Rural polluted	44	11~52 (49)	0~30 (0)	8.4	5.3 ± 1.5	3.0 ± 0.8
04-05/2007	Hohenpeissenber, Germany	47° 48' N, 11° 00' E (980m)	High-elevation forest	46	0~2 (0)	0~5 (0)	4.1	No event	No event
04-05/2007	K-Puszt, Hungary	46° 58' N, 19° 35' E (125m)	Deciduous forest	83	16~79 (72)	0~40 (15)	6.6	5.6 ± 2.4	3.6 ± 1.6
04-05/2007	San Pietro Capofiume, Italy	44° 37' N, 11° 40' E (11m)	Suburban	36	60~97 (89)	0~23 (2)	4.4	4.1 ± 1.4	1.2 ± 0.3
04-05/2007	Finokalia, Greece	35° 20' N, 25° 40' E (250m)	Coastal	15	0~2 (0)	0	4.2	5.9 ± 0.1	No event
03-06/2014	Leicester, UK	52° 37' N, 1° 07' W (375m)	Urban	22	38~57 (56)	0~39 (10)	4.8 ± 1.8	2.9 ± 1.0	1.1 ± 0.4
04-07/2012	Gadanki, India	13.46° N, 79.17° E	Semi-urban	6	0~26 (22)	0	7.1 ± 4.6	4.2 ± 0.5	1.8 ± 3.3
09-11/2015	Nanjing, China	32.30° N, 118.72° E	Urban	22	0~4 (3)	0	40 ± 25 *	14.9 ± 16.5 °	No event
06-07/2014	WangDu, China	38.67° N, 115.21° E	Rural	54	38~92 (88)	0	No observation		
04-05/2010	QingDao, China	36° 09' N, 120° 29' E	Urban/Coast	41	1~10 (10)	0~5 (0)	30.5 ± 12	7.6 ± 2	No event
10-11/2010	HongKong, China	22.40° N, 114.12° E (640m)	Suburban	23	0	0	50~190	3.4 ± 10.2	No event
12/2010-01/2011	HongKong, China	22.3° N, 114.18° E (40m)	Urban	20	0	0	0.63	No event	No event

^aObs represents mean value from observation from measurements

^bThe lower limit of the result from model simulation is derived when choosing the 10th percentile of all smallest nucleation rates as the threshold of NPF event happening, while the upper limit is based on the 90th percentile. Values in brackets represent results obtained using the median as the threshold value.

^cThe condensation sink (CS) is calculated for the entire duration of both the simulation and the measurement period, not solely during new particle formation (NPF) events.

^dMeasurements in Pallas, Hyytiälä, Vavihill, Mace Head, Cabauw, Melpitz, Hohenpeissenber, K-Puszt, San Pietro Capofiume and Finokalia are from Manninen et al. (2010). Others are the same as Table S1.

104

106

108

110

112

Table S3. Comparison of sulfur budget across different studies.

		This study (CESM-MAM4)			Liu et al. (2012)		Spracklen et al. (2005)	Mann et al. (2010)
		Default	Inorg	Inorg_Org	CESM-MAM3	CESM-MAM7	GLOMAP-bin	GLOMAP-mode
Gas Burden (Tg S)	SO ₂	0.29	0.29	0.29	0.35	0.34	0.49	0.3 (0.2-0.68)
	DMS	0.068	0.067	0.067	0.067	0.067	0.04	0.027 (0.02-0.15)
	H ₂ SO ₄	0.0006	0.00059	0.00054	0.0004	0.00042		0.0001
Gas Sink (Tg S/yr)	SO ₂ deposition	27.76	27.76	27.78	19.7	19		
	H ₂ SO ₄ aqueous	0.48	0.49	0.48	0.59	0.51		
	H ₂ SO ₄ condensation	11.61	12.018	11.89	13.9	13.7	13	
	H ₂ SO ₄ deposition	0.0079	0.023	0.016	0.002	0.003	0.01	
	H ₂ SO ₄ nucleation	0.37	0.11	0.17	0.03	0.03	0.07	
Gas Source	H ₂ SO ₄ production	12.57	12.77	12.66	14.5	14.3		
H ₂ SO ₄ lifetime (min)		24.87	24.3	22.44	14.5	15.3		

Table S4. Comparison of H₂SO₄ concentration with measurements

Measurement site	Measurement time	Coordinates	[H ₂ SO ₄] 10 ⁶ molec cm ⁻³ (>10 ⁴)			
			Mean		Median	
			Measurement	Simulation	Measurement	Simulation
Hyytiälä, Finland	24.3.–28.6.2007	61° 51' N, 24° 17' E, 181 m a.s.l.	0.43	2.61	0.18	0.3
San Pietro Capofiume, Italy	21.6.–16.7.2009	44° 39' N, 11° 37' E, 11 m a.s.l.	5.40	4.57	2.40	2.79
Melpitz, Germany	30.4.–31.5.2008	51° 32' N, 12° 54' E, 87 m a.s.l.	6.43	10.53	2.94	2.8
Niwot Ridge, Colorado USA	24.6.–15.7.2007	40° 62' N, 105° 50' W, 3022 m a.s.l.	1.83	2.52	1.40	1.36
Atlanta, Georgia USA	30.7.–31.8.2002	33° 74' N, 84° 38' W, 275 m a.s.l.	12.90	9.95	2.85	1.03
Beijing, China	1.6–31.8.2008	four-layer building in THU 40° 94' N, 116° 33' E	2.51	17.91	1.81	3.15

130 **References**

- 132 Chung, S. H. and Seinfeld, J. H.: Global distribution and climate forcing of carbonaceous aerosols, *J. Geophys. Res.-*
Atmos., 107, 10.1029/2001jd001397, 2002.
- 134 Dai, L., Wang, H., Zhou, L., An, J., Tang, L., Lu, C., Yan, W., Liu, R., Kong, S., Chen, M., Lee, S., and Yu, H.:
Regional and local new particle formation events observed in the Yangtze River Delta region, China, *J. Geophys.*
136 *Res.-Atmos.*, 122, 2389-2402, 10.1002/2016jd026030, 2017.
- 138 Franchin, A., Ehrhart, S., Leppä, J., Nieminen, T., Gagné, S., Schobesberger, S., Wimmer, D., Duplissy, J.,
Riccobono, F., Dunne, E. M., Rondo, L., Downard, A., Bianchi, F., Kupc, A., Tsagkogeorgas, G., Lehtipalo, K.,
Manninen, H. E., Almeida, J., Amorim, A., Wagner, P. E., Hansel, A., Kirkby, J., Kürten, A., Donahue, N. M.,
140 Makhmutov, V., Mathot, S., Metzger, A., Petäjä, T., Schnitzhofer, R., Sipilä, M., Stozhkov, Y., Tomé, A.,
Kerminen, V. M., Carslaw, K., Curtius, J., Baltensperger, U., and Kulmala, M.: Experimental investigation of ion-
142 ion recombination under atmospheric conditions, *Atmos. Chem. Phys.*, 15, 7203-7216, 10.5194/acp-15-7203-2015,
2015.
- 144 Guo, S., Hu, M., Zamora, M. L., Peng, J. F., Shang, D. J., Zheng, J., Du, Z. F., Wu, Z., Shao, M., Zeng, L. M.,
Molina, M. J., and Zhang, R. Y.: Elucidating severe urban haze formation in China, *P. Natl. Acad. Sci. USA.*, 111,
146 17373-17378, 10.1073/pnas.1419604111, 2014.
- 148 Hama, S. M. L., Ma, N., Cordell, R. L., Kos, G. P. A., Wiedensohler, A., and Monks, P. S.: Lung deposited surface
area in Leicester urban background site/UK: Sources and contribution of new particle formation, *Atmos. Environ.*,
151, 94-107, <https://doi.org/10.1016/j.atmosenv.2016.12.002>, 2017.
- 150 Herrmann, E., Ding, A. J., Kerminen, V. M., Petäjä, T., Yang, X. Q., Sun, J. N., Qi, X. M., Manninen, H., Hakala,
J., Nieminen, T., Aalto, P. P., Kulmala, M., and Fu, C. B.: Aerosols and nucleation in eastern China: first insights
152 from the new SORPES-NJU station, *Atmos. Chem. Phys.*, 14, 2169-2183, 10.5194/acp-14-2169-2014, 2014.
- 154 Kanawade, V. P., Tripathi, S. N., Siingh, D., Gautam, A. S., Srivastava, A. K., Kamra, A. K., Soni, V. K., and Sethi,
V.: Observations of new particle formation at two distinct Indian subcontinental urban locations, *Atmos. Environ.*,
96, 370-379, <https://doi.org/10.1016/j.atmosenv.2014.08.001>, 2014.
- 156 Kontkanen, J., Järvinen, E., Manninen, H. E., Lehtipalo, K., Kangasluoma, J., Decesari, S., Gobbi, G. P., Laaksonen,
A., Petäjä, T., and Kulmala, M.: High concentrations of sub-3nm clusters and frequent new particle formation
158 observed in the Po Valley, Italy, during the PEGASOS 2012 campaign, *Atmos. Chem. Phys.*, 16, 1919-1935,
10.5194/acp-16-1919-2016, 2016.
- 160 Liu, X., Easter, R. C., Ghan, S. J., Zaveri, R., Rasch, P., Shi, X., Lamarque, J. F., Gettelman, A., Morrison, H., Vitt,
F., Conley, A., Park, S., Neale, R., Hannay, C., Ekman, A. M. L., Hess, P., Mahowald, N., Collins, W., Iacono, M.
162 J., Bretherton, C. S., Flanner, M. G., and Mitchell, D.: Toward a minimal representation of aerosols in climate
models: description and evaluation in the Community Atmosphere Model CAM5, *Geosci. Model Dev.*, 5, 709-739,
164 10.5194/gmd-5-709-2012, 2012.
- 166 Mann, G. W., Carslaw, K. S., Spracklen, D. V., Ridley, D. A., Manktelow, P. T., Chipperfield, M. P., Pickering, S.
J., and Johnson, C. E.: Description and evaluation of GLOMAP-mode: a modal global aerosol microphysics model
for the UKCA composition-climate model, *Geosci. Model Dev.*, 3, 519-551, 10.5194/gmd-3-519-2010, 2010.
- 168 Manninen, H. E., Nieminen, T., Asmi, E., Gagné, S., Häkkinen, S., Lehtipalo, K., Aalto, P., Vana, M., Mirme, A.,
Mirme, S., Hörrak, U., Plass-Dülmer, C., Stange, G., Kiss, G., Hoffer, A., Törö, N., Moerman, M., Henzing, B., de
170 Leeuw, G., Brinkenberg, M., Kouvarakis, G. N., Bougiatioti, A., Mihalopoulos, N., O'Dowd, C., Ceburnis, D.,
Arneth, A., Svenningsson, B., Swietlicki, E., Tarozzi, L., Decesari, S., Facchini, M. C., Birmili, W., Sonntag, A.,
172 Wiedensohler, A., Boulon, J., Sellegri, K., Laj, P., Gysel, M., Bukowiecki, N., Weingartner, E., Wehrle, G.,
Laaksonen, A., Hamed, A., Joutsensaari, J., Petäjä, T., Kerminen, V. M., and Kulmala, M.: EUCAARI ion
174 spectrometer measurements at 12 European sites – analysis of new particle formation events, *Atmos. Chem. Phys.*,
10, 7907-7927, 10.5194/acp-10-7907-2010, 2010.
- 176 Meng, H., Zhu, Y., Evans, G. J., Jeong, C.-H., and Yao, X.: Roles of SO₂ oxidation in new particle formation
events, *J. Environ. Sci.*, 30, 90-101, <https://doi.org/10.1016/j.jes.2014.12.002>, 2015.
- 178 Pierce, J. R., Riipinen, I., Kulmala, M., Ehn, M., Petäjä, T., Junninen, H., Worsnop, D. R., and Donahue, N. M.:
Quantification of the volatility of secondary organic compounds in ultrafine particles during nucleation events,
180 *Atmos. Chem. Phys.*, 11, 9019-9036, 10.5194/acp-11-9019-2011, 2011.
- 182 Spracklen, D. V., Pringle, K. J., Carslaw, K. S., Chipperfield, M. P., and Mann, G. W.: A global off-line model of
size-resolved aerosol microphysics: I. Model development and prediction of aerosol properties, *Atmos. Chem.*
Phys., 5, 2227-2252, 10.5194/acp-5-2227-2005, 2005.

184 Wang, Z. B., Hu, M., Pei, X. Y., Zhang, R. Y., Paasonen, P., Zheng, J., Yue, D. L., Wu, Z. J., Boy, M., and
186 Wiedensohler, A.: Connection of organics to atmospheric new particle formation and growth at an urban site of
188 Beijing, *Atmos. Environ.*, 103, 7-17, 10.1016/j.atmosenv.2014.11.069, 2015.
190 Wu, Z. J., Ma, N., Groß, J., Kecorius, S., Lu, K. D., Shang, D. J., Wang, Y., Wu, Y. S., Zeng, L. M., Hu, M.,
192 Wiedensohler, A., and Zhang, Y. H.: Thermodynamic properties of nanoparticles during new particle formation
194 events in the atmosphere of North China Plain, *Atmos. Res.*, 188, 55-63,
196 <https://doi.org/10.1016/j.atmosres.2017.01.007>, 2017.
198 Yu, H., Ortega, J., Smith, J. N., Guenther, A. B., Kanawade, V. P., You, Y., Liu, Y., Hosman, K., Karl, T., Seco, R.,
200 Geron, C., Pallardy, S. G., Gu, L., Mikkilä, J., and Lee, S.-H.: New Particle Formation and Growth in an Isoprene-
Dominated Ozark Forest: From Sub-5 nm to CCN-Active Sizes, *Aerosol Sci. Technol.*, 48, 1285-1298,
10.1080/02786826.2014.984801, 2014.
Zhang, Y. M., Zhang, X. Y., Sun, J. Y., Lin, W. L., Gong, S. L., Shen, X. J., and Yang, S.: Characterization of new
particle and secondary aerosol formation during summertime in Beijing, China, *Tellus B.*, 63, 382-394,
10.1111/j.1600-0889.2011.00533.x, 2011.
Zhu, Y., Sabaliauskas, K., Liu, X., Meng, H., Gao, H., Jeong, C.-H., Evans, G. J., and Yao, X.: Comparative
analysis of new particle formation events in less and severely polluted urban atmosphere, *Atmos. Environ.*, 98, 655-
664, <https://doi.org/10.1016/j.atmosenv.2014.09.043>, 2014.